Metrol. Meas. Syst., Vol. 31 (2024), No. 4
DOI: 10.24425/mms.2024.152047

METROLOGY AND MEASUREMENT SYSTEMS
Index 330930, ISSN 0860-8229
www.metrology.wat.edu.pl

EDDY CURRENT-BASED MEASUREMENT SYSTEM FOR EVALUATING FIBER DISTRIBUTION TO PREDICT CRACKS IN STEEL FIBER-REINFORCED CONCRETE: EXPERIMENTAL STUDY

Loukmane Gherdaoui[1)], Samir Bensaid[1)], Nacira Saoudi[2)], Didier Trichet[3)], Hamza Houassine[4)]

1) *Laboratoire Des Matériaux Et Du Développement Durable (LM2D), Sciences and Applied Sciences Faculty, Algeria* (✉ *l.gherdaoui@univ-bouira.dz*)
2) *Civile Engineering Department, Sciences and Applied Sciences Faculty, Bouira University, Algeria*
3) *Nantes Université, Institut de Recherche en Energie Electrique de Nantes Atlantique, IREENA, UR 4642, 44600 Saint-Nazaire, France*
4) *Laboratoire d'Ingénierie des Systèmes Electriques et Automatiques,, Sciences and Applied Sciences Faculty, Bouira University, Algeria*

Abstract

This paper presents a non-destructive approach for evaluating steel fiber distribution in Steel Fiber Reinforced Concrete (SFRC). The method utilizes a measurement system, based on eddy currents combined with an automated scanning system, enabling precise sensor movements along the SFRC sample. The proposed method is first applied on a set of samples with known fiber distribution along the samples, in order to test its effectiveness. The impedance response clearly indicates the highest and lowest fiber volume fractions along the samples, allowing for a straightforward correlation between the impedance data and fiber distribution through the established methodology. Then it is applied to another set of samples with random fiber distribution. In this case, the impedance response is compared to the Brazilian destructive test results. The obtained results affirm a robust correlation between impedance measurements and the observed cracks on the SFRC samples. This approach proves instrumental in identifying vulnerable areas susceptible to crack development within the SFRC sample. The comprehensive insights gained through this method contribute significantly to show the detailed zonal distribution of SFRC which allow understanding the behavior of the SFRC under mechanical stress.

Keywords: Steel Fiber-Reinforced Concrete, Eddy Current Non-Destructive Evaluation, Fiber Distribution, Linear Scan System, Brazilian Test, Crack Predicting.

1. Introduction

Steel Fiber-Reinforced Concrete (SFRC) is an efficient construction material used in various applications such as dam construction, tunnel Lining, and concrete pipe [1]. Incorporating steel fibers into concrete benefits its tensile strength, enhancing structural member's ability to carry significant stresses and absorb more energy, providing superior resistance to cracking and crack propagation by acting as a bridge to absorb stress forces, this bridging action helps distribute stress across potential cracks, thus preventing their formation and propagation. [2-4]. During the construction of SFRC, the spatial distribution of fibers is non-uniform, characterized by a randomly anisotropic nature [5, 6]. This randomness in distribution significantly affects the mechanical properties of SFRC [7, 8]. When fibers are randomly distributed, it results in lower fiber content in specific zones within the concrete. This decrease in fiber content leads to reduced efficiency of SFRC in those particular areas. Furthermore, their ability to reinforce concrete is substantially compromised when fibers are aligned perpendicular to the direction of tensile stress. [9, 10]. Hence, to assess the efficiency and mechanical performance of SFRC, evaluating the distribution of steel fibers within the concrete matrix is crucial. Understanding

Article history: received March 9, 2024; revised July 12, 2024; accepted July 16, 2024; available online September 17, 2024.

how these fibers are dispersed provides essential insights into the material's overall strength, durability, and ability to resist various mechanical forces.

The evaluation of fiber distribution and dispersion in SFRC can be accomplished through various methods. One of the most effective *non-destructive* (ND) techniques employed for evaluating the internal structure of *Steel Fiber Reinforced Concrete* (SFRC) is the X-ray computed tomography method [11-13]. This technique yields a clear image, enabling a comprehensive analysis of the fiber distribution within the SFRC by providing high-resolution, three-dimensional images that allow for detailed visualization and examination of the fiber distribution within the concrete matrix. Another approach, considered a destructive method, involves applying image processing techniques [14, 15] to the cross-sectional areas of the samples. A photograph of a section of a concrete sample is taken, and the coordinates of fibers are determined using a software tool. This method provides detailed quantitative data on fiber distribution, although it requires physically cutting the sample, which destroys the test specimen. The impedance spectroscopy (AC-IS) [16] has also been considered. This electrical method uses alternative current with various frequency ranges to determine the current transfer function of the specimen. The authors in [17] introduce an alternative ND method, relying on measuring magnetic properties. This approach involves a ferrite magnetic circuit, where the concrete sample serves as the closure yoke for the circuit, necessitating direct contact with the samples.

Stephan Van Damme *et al.* [18] presented a microwave nondestructive testing technique using an open-ended coaxial probe reflectometry method. This method is employed for measuring the effective permittivity of steel fiber-reinforced concrete and applies a classical homogenization approach to determine the fiber content.

The authors in [19] highlighted an electrical contact non-destructive method. This approach involves measuring the anisotropic conductivity of SFRC under a DC voltage. Notably, the method exhibits high sensitivity to humidity and temperature.

A non-destructive method based on the electromagnetic induction phenomenon has been presented by [20-22]. This approach involves employing an inductor coil supplied with AC voltage. The estimation of the fiber dispersion in the specimen is achievable through monitoring changes in the coil inductance. The change in coil impedance is proportional to the fiber volume content in the sample. Additionally, it is sensitive to the orientation of the fibers; the closer the fibers are oriented to the direction of the magnetic field, the higher the impedance.

While the methods described in the cited papers show promising results, it's important to highlight that the evaluation of fiber distribution is global and lacks detailed insights into all tested sample zones. To remedy this drawback, one proposes non-destructive method to establish a refined zonal distribution map using measurement system based on Eddy Currents combined to a scan system with a motorized coil displacement, along the test samples.

The main aim of the proposed method is to predict cracks by evaluating the zonal distribution of fibers in samples of SFRC using the measurement system based on eddy currents.

The proposed system is entirely controlled by LabVIEW software. It consists of linear displacement axis and impedance measurement process. The linear displacement axis securely holds the *eddy current sensor* (ECS), allow positioning it accurately at specific location along the sample. Sequentially the LabVIEW direct the LCR meter to measure the sample impedance at each designated position. The process continues until all positions of the tested sample are measured.

The proposed method is first applied to SFRC samples intentionally prepared with a known zonal fiber distribution in order to validate its effectiveness in precisely detecting the fiber volume fraction distribution along the sample. The ECS impedance change will be used as indicator for the fiber volume fraction, facilitating the distinct identification of each zone from another. Secondly, the proposed method is extended to a set of samples with unknown fiber

distribution, with a naturally random fiber distribution. The measured impedance for all samples is correlated to the Brazilian destructive tests. This test aimed to assess the post-cracking properties of the SFRC, providing valuable insights into the material and structural behavior under loading conditions.

2. Measurement setup description

The eddy current-based measurement system, dedicated for evaluation of the fiber distribution of SFRC samples (Fig. 1), consists of:

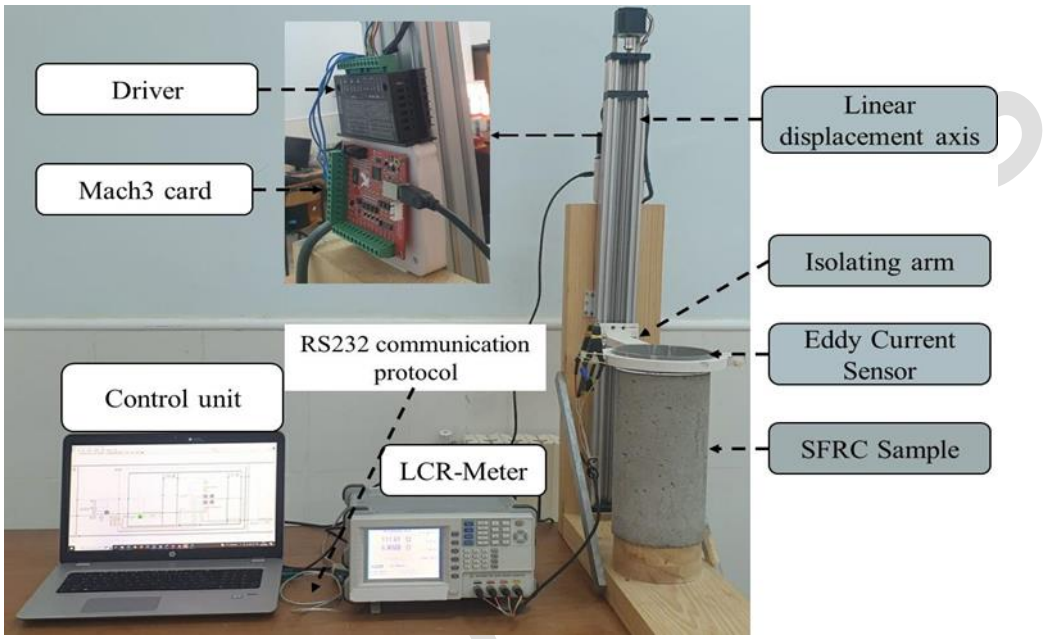

Fig. 1. Measurement system based on Eddy Currents combined with to a scanning system.

a. **SFRC Sample:** The SFRC sample used in the characterization is cylindrical, with a diameter of 160 mm and a height of 320 mm. The used steel fibers are of the hooked end type, with a diameter of 0.54 mm and a length of 37.7 mm, while the proprietary electromagnetic properties are presented in [23].

b. **LCR-Meter:** An LCR-meter (GW INSTEK/ LCR-8105G), controlled by a computer using LabVIEW software via RS232 protocol, is employed to measure the impedance of the SFRC sample, enabling precise and automated measurements.

c. **Eddy Current Sensor (ECS):** consist of a single-layered coil with 35 turns supported by a cylindrical PVC container, adapted to the dimensions of the SFRC sample, as illustrated in Fig. 2.

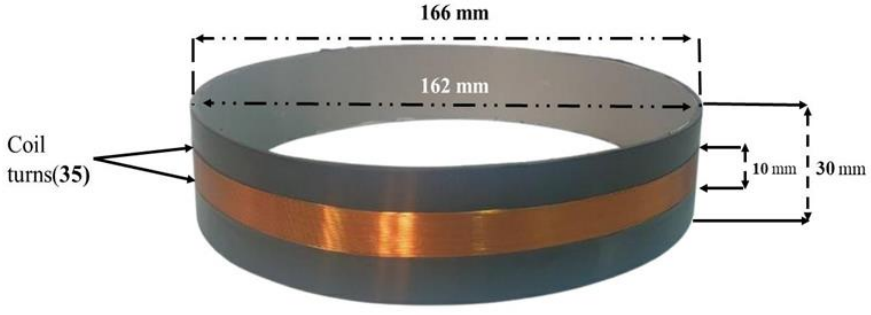

Fig. 2. Eddy current sensor (ECS) dimensions.

d. **Displacement System:** a displacement system, responsible for moving the arm that hold the sensor measuring the impedance along the SFRC sample, comprises the following components:

- **Linear Displacement Axis**: consists of a precision Stepper Motor assigned to move the arm, providing precise control over its positioning, a C Beam offering structural support, and a Lead Screw converting rotary motion into controlled linear movement along the SFRC sample.
- **Isolating Arm:** The arm holding the sensor is constructed from insulating material (wood), preventing the magnetic induction from interference.
- **Control System:** The control system consists of Mach3 card with USB connection controller unit, enabling seamless and precise command of the stepper motor. Mach3 receives commands and instructions from the controller unit through LABVIEW and translates them into signals for the driver.
- **Driver:** The driver serves as an intermediary between the control card and the stepper motor, translating signals from the command card into specific pulses series for the stepper motor.
- **Power Supply:** The power supply provides a stable 12V output with sufficient current, delivering the necessary electrical energy to operate the displacement system.

The Eddy Current Non-Destructive scan system is entirely performed and controlled using LabVIEW software. It receives and manages commands related to ECS displacement, communicates with the LCR meter to initiate measurements, and processes the acquired data. This integrated approach enhances automation, accuracy, and real-time parameter adjustment for the impedance measurement.

3. Proposed method operation algorithm

The proposed method employs eddy current non-destructive evaluation technique. The SFRC sample placed within ECS which consist of encircled coil supplied by an alternating low voltage. The coil traversed by an electrical current generates a variable magnetic field which induces currents in the steel fibers, which in turn create an opposing magnetic field that interferes with the source field. Measuring the variation in the coil impedance (Ratio of voltage and current vectors) allows for assessing how steel fibers are distributed within the cementitious matrix.

In order to assess the fiber dispersion along the SFRC sample, the ECS impedance is measured for each step displacement along the sample.

Figure 3 illustrates operation algorithm of the Eddy Current Non-Destructive scan system. At position 0 mm, the controlling system directs the LCR meter to measure the real and imaginary parts of impedance. Subsequently, the stepper motor is controlled using mach3 card to displace the ECS by 1 mm. Following the displacement, the LCR meter is again controlled to measure impedance. This process repeated iteratively until the position reaches 360 mm. Once the position reaches 360 mm, the controlling system directs the stepper motor to return to the starting position at 0 mm.

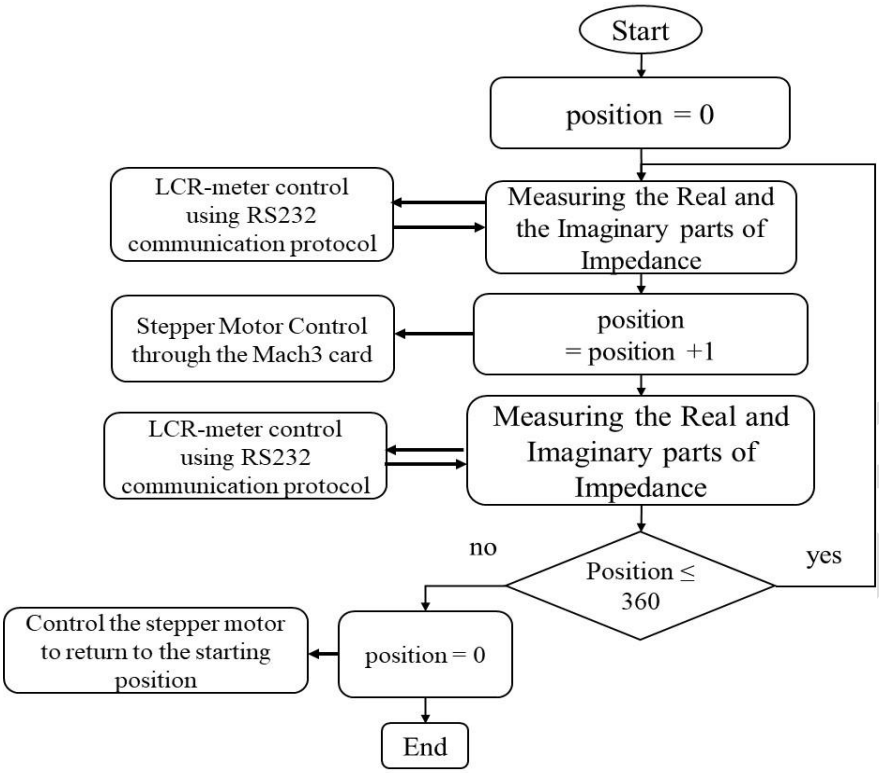

Fig. 3. Operation algorithm of the Eddy Current Non-Destructive scan system.

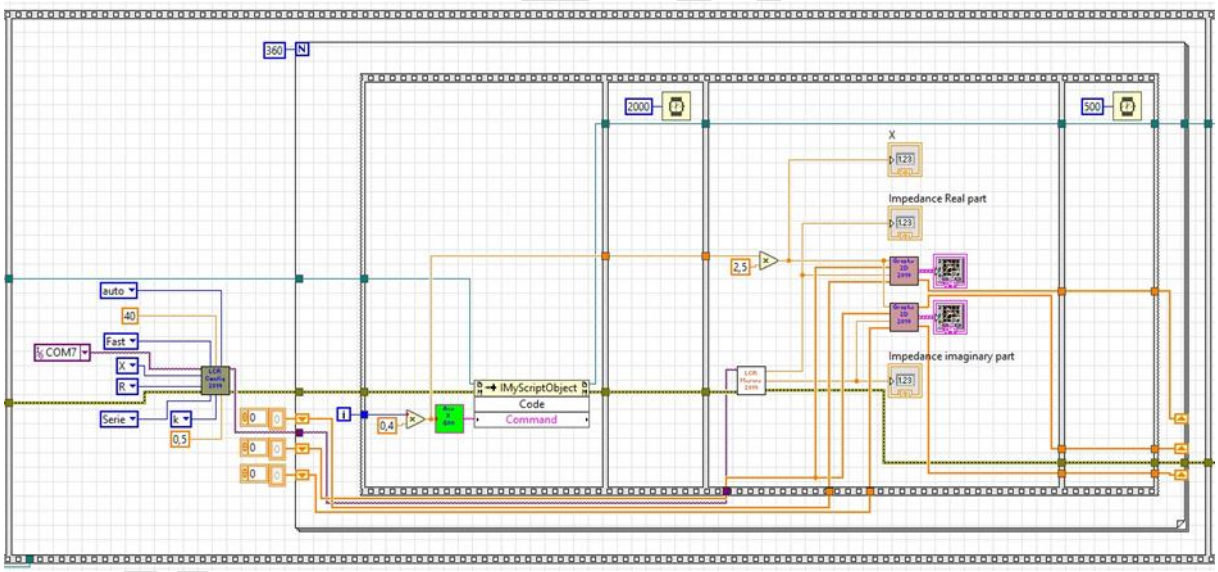

Fig. 4. LabVIEW Block Diagram.

Figure 4 displays the LabVIEW Block Diagram which reproduces the algorithm (Fig. 3), allowing ECS measurement and displacement along the SFRC sample. The diagram incorporates loops for iterative control, ensuring sequential impedance measurements and precise ECS displacement.

4. Choose of the working frequency and sensitive impedance part

The effects of induced current in the steel fiber begin to appear when the skin depth δ is smaller than the fiber radius, where is computed as following:

$$\delta = \sqrt{\frac{\rho}{\pi f \mu}} \tag{1}$$

Where: ρ, μ are successively the electrical resistivity the magnetic permeability of the steel fiver and f is the frequency of the source current.

as illustrated in figure 5, depicting the ratio of skin depth on the fiber radius (0.27mm) for values below 1 (12kHz) After 12 kHz, the real part of impedance increases and the imaginary part decreases when the frequency increases. Less than 12 kHz the real part variation is practically negligible, while the imaginary part variation is slightly noticeable. Beyond 12 kHz, as indicated in Fig. 5, the decision to operate at frequencies above 12 kHz becomes imperative.

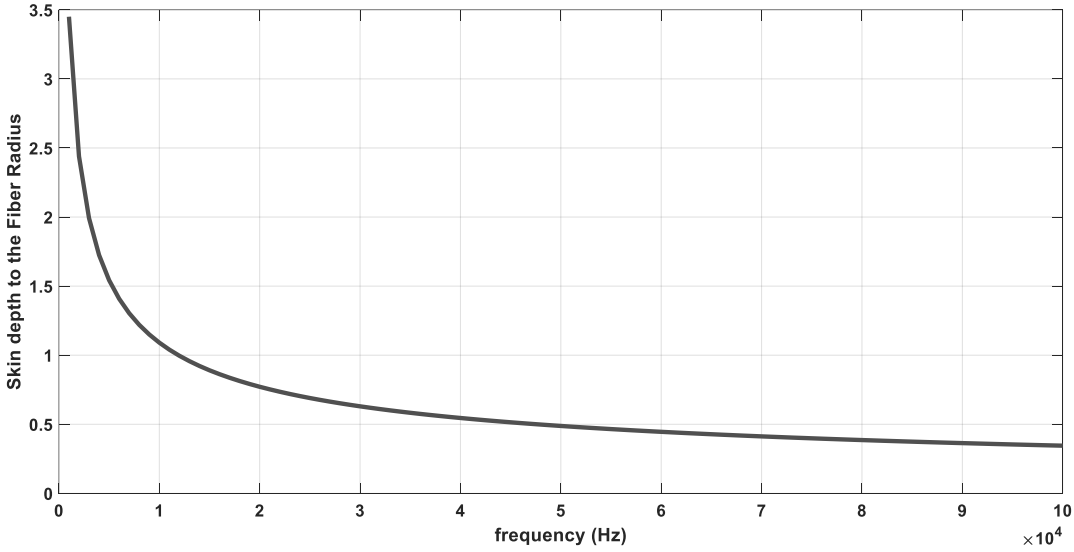

Fig. 5. Ratio of the Skin thickness on the fiber radius according to the frequency.

To determine the working frequency, as well as the impedance part that is sensitive to the presence of steel fiber, a multiple impedance measurements were conducted through frequency sweep ranging from 100 Hz to 1 MHz) on one sample. One has limited the frequency to 1 MHz to avoid the capacitive effects in the ECS [23].

Figure 6 represents the real part of impedance variation of SFRC sample according to frequency. The relative variation of the impedance part of SFRC sample is computed as:

$$\Delta Z = \frac{Z_{SFRC} - Z_{void}}{Z_{void}} \times 100, \tag{2}$$

where: ΔZ, Z_{SFRC}, Z_{void} are successively the ECS impedance part change, the impedance part with SFRC and The impedance part without SFRC.

Metrol. Meas. Syst., Vol. 31 (2024), No. 4
DOI: 10.24425/mms.2024.152047

a) Real part b) Imaginary part

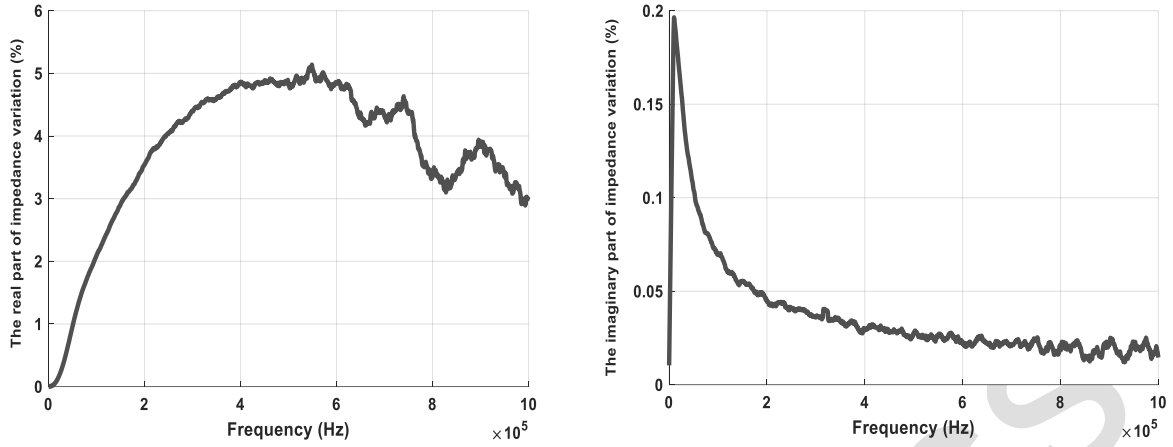

Fig. 6. Relative variation impedance parts according to frequency.

Figures 6a and 6b show respectively the relative variation of the real and the imaginary parts of the impedance on the presence of the SFRC. While the imaginary part is sensitive at low frequencies, the real part is more sensible at the high frequencies. The variation in the imaginary part is 24th less than the real part. Thus real part is more sensitive than the imaginary part. Hence, the impedance real part is chosen as the indicator parameter in the proposed method.

The maximal relative variation of the impedance real part (Fig. 6a) highest in the frequency range of 38 kHz to 62kHz. Therefor the frequency 40kHz is chosen as a working frequency at which the ECS intercepts a significant impedance variation with a highest sensitive to the presence of steel fiber.

5. Applications of the proposed method

5.1. Application on a set of known fiber distribution samples

The proposed non-destructive assessment method is first applied to SFRC samples intentionally prepared with known zonal fiber distribution in order in order to test its effectiveness in precisely detecting the fiber volume fraction distribution along the sample. The ECS Real Impedance Part Changes (Eq. 2) will be used as indicator for fiber volume fraction, facilitating the distinct identification of each zone from another. These preliminary tests aimed to establish a baseline for understanding how impedance changes relate to different fiber volume fractions.

These samples have been meticulously designed to exhibit well-determined volume fractions of fibers within specific zones. One prepared two samples with various zones with deferent steel fiber volume fractions. Notably, each sample overall volume fraction of steel fibers is maintained at a consistent 1%, as illustrated in Fig. 7a and Fig. 7b.

The samples were demolded after 36h, and afterwards the samples were placed into a curing chamber devoid of humidity for 28days in preparation for the tests. Following the curing period, the impedance of each sample is measured.

The mixture composition of SFRC specimens for Sample 1 and Sample 2 is detailed in Table 1.

Table 1. Mixture composition of SFRC samples 1 and 2.

Samples	Cement (kg/m³)	Water (liter/m³)	Sand 0/3 (kg/m³)	Superplasticizer (liter)	Sample Steel Fiber Volume Fraction
Sample 1	350	160	1350	3	1%
Sample 2	350	160	1350	3	1%

The Eddy Current Non-Destructive scan system will be employed to measure the real part of the impedance variation at various positions along the samples.

Figure 8 illustrates the real part of impedance relative variation according to ECS Position. The ECS input position in the figure represents the location where the sensor enters the specimen, while the ECS output position denotes the location where the sensor exits the sample. Dashed lines represent the positions of the boundaries of each zone within the sample.

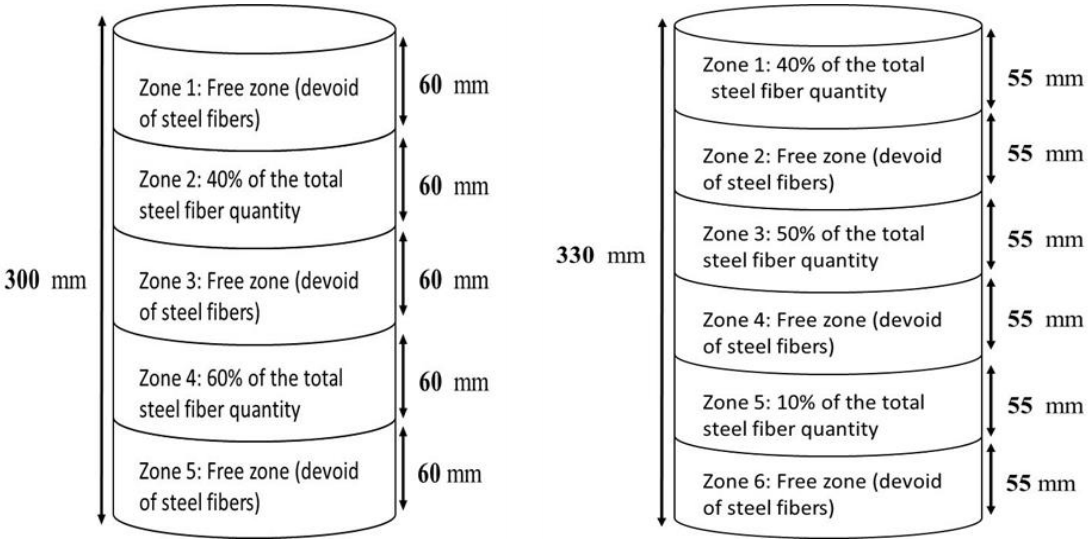

Fig. 7. Zonal Distribution of Steel Fibers in Sample 1 and sample 2.

Notably, areas with low coil impedance result from one of two conditions: a deficiency of fibers in the area or the poor placement of fibers, which are perpendicular to the magnetic field vector.

As illustrated in the Fig. 8, the ECS initiates entry into Zone 1 at a position of 0 mm. The relative variation of the impedance real part in Zone 1 reveals null values, correlating with the absence of fibers in this zone. Moving to the second zone (60 mm), we observe an increase in impedance variation attributed to the presence of steel fibers (0.4 of the total quantity), reaching values of 4%.

Upon entering Zone 3 at 120 mm, a noticeable decrease in impedance occurs due to the absence of fibers, reaching values of 1%. As the ECS progresses to 180 mm, entering Zone 4, there is an increase in impedance, reaching values of 7%, reflecting the presence of steel fibers (0.6 of the total quantity). Notably, the maximum impedance values in Zone 4 surpass those in Zone 2, as expected due to a higher fiber presence in Zone 4.

At the ECS entry into Zone 5 at 240 mm, a decrease in impedance is observed, aligning with the absence of fibers and reaching approximate values of 0. Importantly, impedance measurement results correlate well with the known fiber distributions. Lower impedance values consistently align with zones lacking steel fibers.

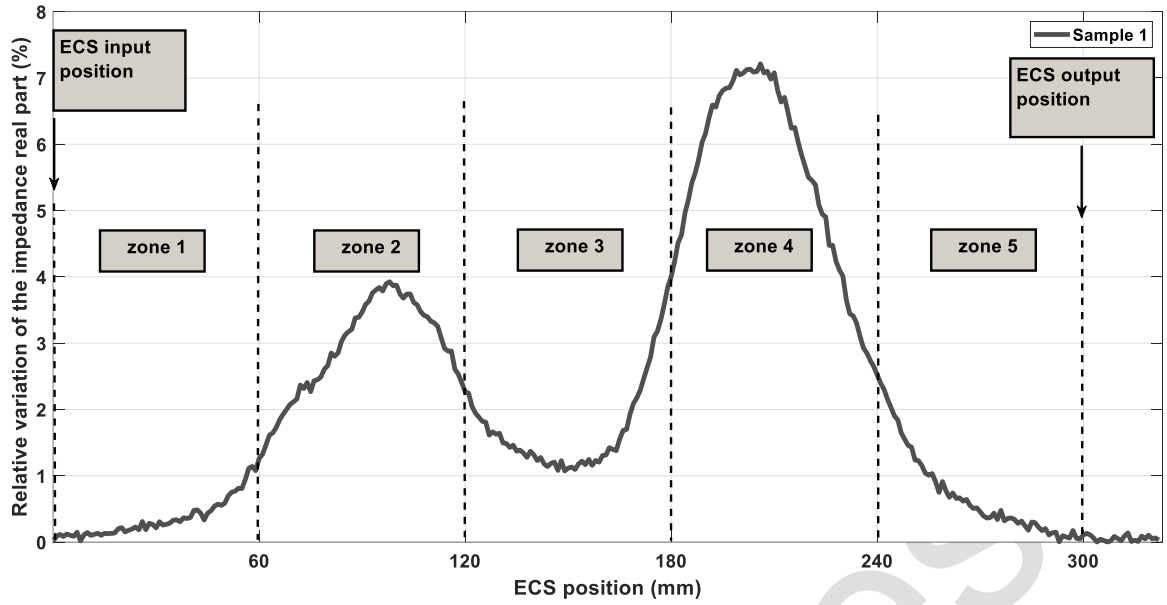

Fig. 8. ECS Impedance Real Part Changes with the SFRC sample 1 according to ECS position.

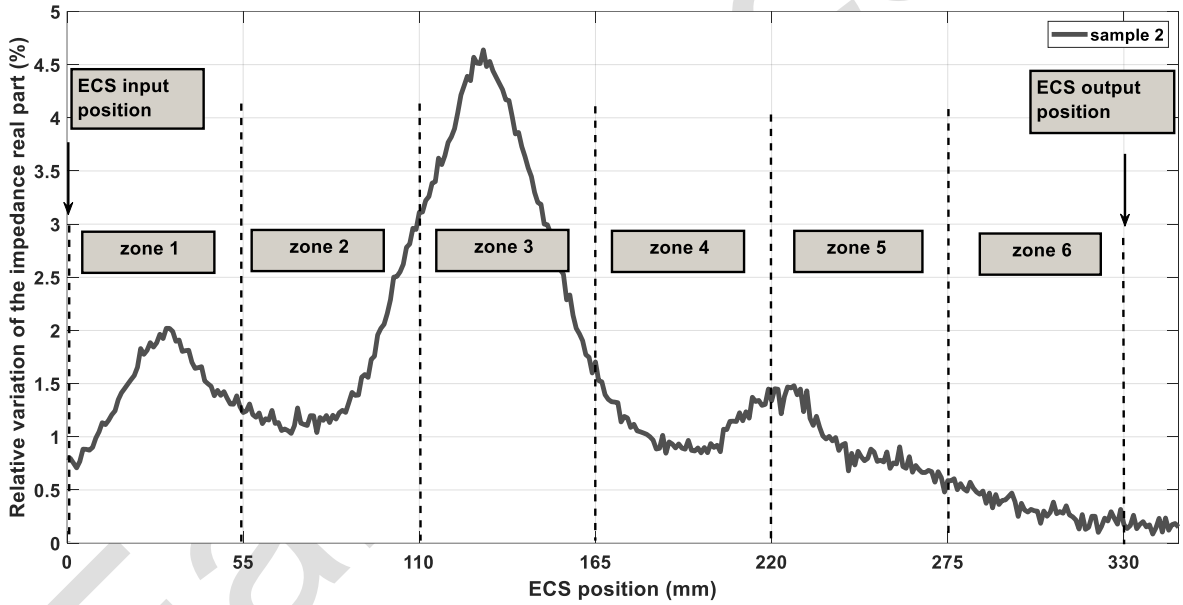

Fig. 9. ECS Impedance Real Part Changes with the SFRC sample 2 according to ECS position.

As illustrated in Fig. 9, the ECS initiates entry into Zone 1 at a position of 0 mm. The real part of the relative impedance in Zone 1 reaches values of 2%, attributed to the presence of steel fibers (0.4 of the total quantity). Moving to the second zone (55 mm), one perceives a decrease in impedance due to the absence of steel fibers, reaching values of 1%. Upon entering Zone 3 at 110 mm, a noticeable increase in impedance occurs, attributed to the presence of fibers (0.6 of the total quantity), reaching values of 4.7%. As the sensor progresses to 165 mm, entering Zone 4, there is an obvious decrease in impedance, reaching values of 0.8%, due to the absence of steel fibers. At the ECS entry into Zone 5 at 220 mm, a little increase in impedance aligns with the presence of fibers (0.1 of the total steel fiber quantity) to reach values of 1.5%. Finally, when the ECS enters Zone 6 at 275 mm position, one observes a decrease in impedance to 0.2%, aligning with the absence of fibers in this zone. One clearly notices that lower impedance values consistently align with zones lacking steel fibers.

In conclusion, the impedance response shows clearly the highest and lowest fiber volume fractions along the samples, thus the correlation between fiber distribution and the impedance value is feasible.

5.2. Application on a set of samples with unknown fiber distribution samples

The proposed method is extended to a set of samples with a naturally random fiber distribution which are unknown. The objective of this part, is to evaluate the efficacy of the proposed method in situations where the fiber distribution is not pre-determined or known. In this case, the destructive method is employed to show the eventual vulnerable zones of the samples, which should be also shown by the measured impedance.

Fig. 10. Set of samples with random fiber distribution.

A set of 33 SFRC samples (Fig. 10) are meticulously prepared and organized into five distinct groups within each group (Table 2). The fibers were meticulously prepared in a one mix with a volume fraction of 1% for each group. The mixture composition of the samples is detailed in Table 2.

Table 2. Mixture Composition of the 33 SFRC Samples.

GROUP	**A**	**F1**	**F2**	**F3**	**F4**
Number of samples	5	7	7	7	7
Cement (kg /m³)	400	400	400	400	400
Water (liter /m³)	140	160	160	160	160
Sand 0/3 (kg/m³)	623	623	623	623	623
Coarse Aggregate (kg/m³) 3/8	243	243	243	243	243
Coarse Aggregate (kg/m³) 8/15	881	881	881	881	881
Superplasticizer ADVA flow liter	4	4	4	4	4
Group Steel Fiber Volume Fraction	1%	1%	1%	1%	1%

The sample groups F1, F2, F3 and F4 are identical in terms of content as indicated in Table 2. The fiber-reinforced concrete for each group is prepared separately. Thus, the difference between the samples in each group is distinguished by the naturally random distribution of fibers.

The samples were demolded after 36 h, and afterwards they were placed into a curing chamber devoid of humidity for 28 days in preparation for the tests. Following the curing period, the Eddy Current Non-Destructive scan system is applied to each sample where the ECS real part of impedance is measured. Then, in order to correlate these non-destructive measurements, the Brazilian destructive tests (Fig. 11) which are commonly used to indirectly measure the tensile strength of materials like SFRC, provides insights into how the fibers are

distributed within the sample, are conducted on all samples. These tests aim to assess the post-cracking properties of the SFRC, providing valuable insights into the material and structural behavior under the loading conditions.

The Brazilian destructive tests involve subjecting a cylindrical SFRC specimen to longitudinal loading, leading to breaks approximately in the chord plane and causing the development of tensile stresses perpendicular to the loading direction. Small cracks can develop as a result around perpendicular to the axis of the cylindrical samples.

Fig. 11. A SFRC sample at time of Brazilian destructive test.

After conducting Brazilian destructive tests on 33 samples, cracks developed and occurred only in 3 samples, namely A1, F1(7), and F2(4). These cracks, which appear approximately perpendicular to the axis of the cylindrical samples reveal important information about the internal fiber distribution.

We know that steel fibers enhance the resistance to tension and compression, acting like a bridge to absorb stress forces. This bridging action helps to transfer stress across potential cracks, thereby preventing their formation and propagation. As a result, the areas where fibers are homogeneously distributed will show more resistance to crack development, resulting in no visual cracks as in the case of the other 30 samples. In contrast, zones with insufficient fiber content are more susceptible and vulnerable to cracking. By analyzing the pattern and extent of these cracks, one can evaluate fiber dispersion within the concrete.

Figure 12 presents SFRC sample A1 after undergoing the Brazilian destructive test, where a ruler measures the crack from the top of the specimen. It is observed that the crack is located at a distance of 195mm from the top.

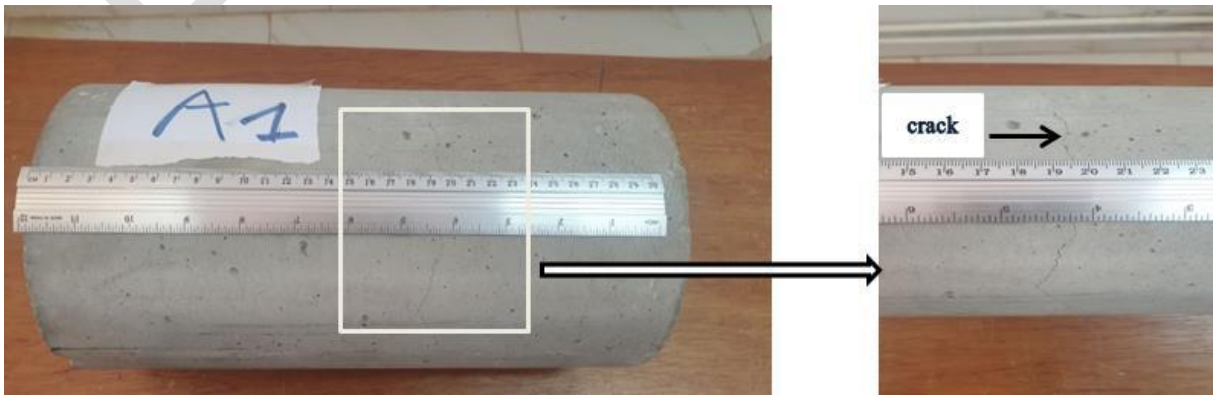

Fig. 12. SFRC sample A1 after undergoing the Brazilian destructive test.

Figure 13 illustrates the exact course of the crack in SFRC sample A1, which occurred approximately perpendicular to the axis of the cylindrical sample. The measured length of the crack is 22.5 cm.

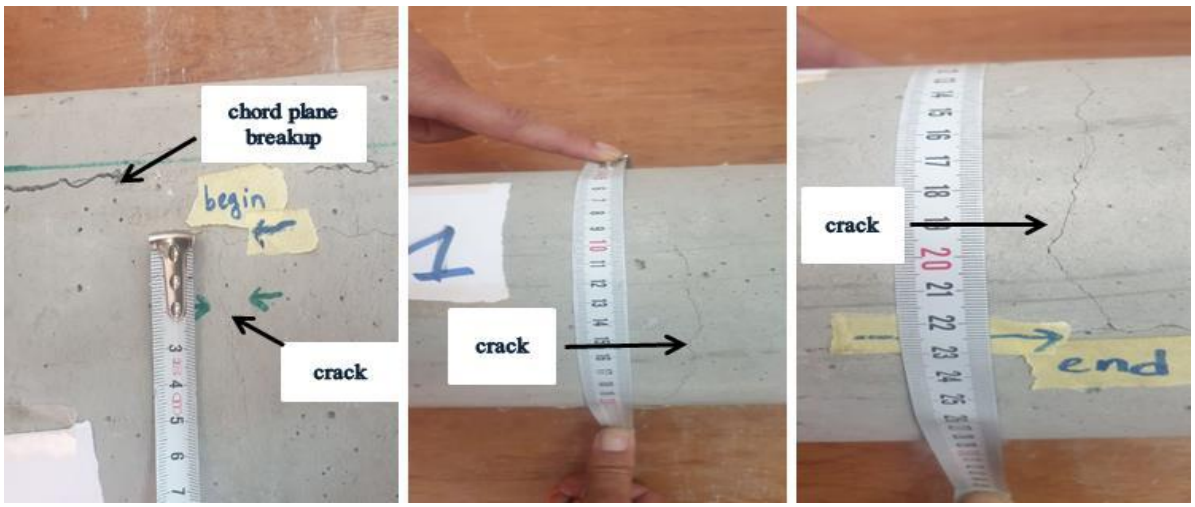

Fig. 13. The Course and Length of the Crack in SFRC Sample A1.

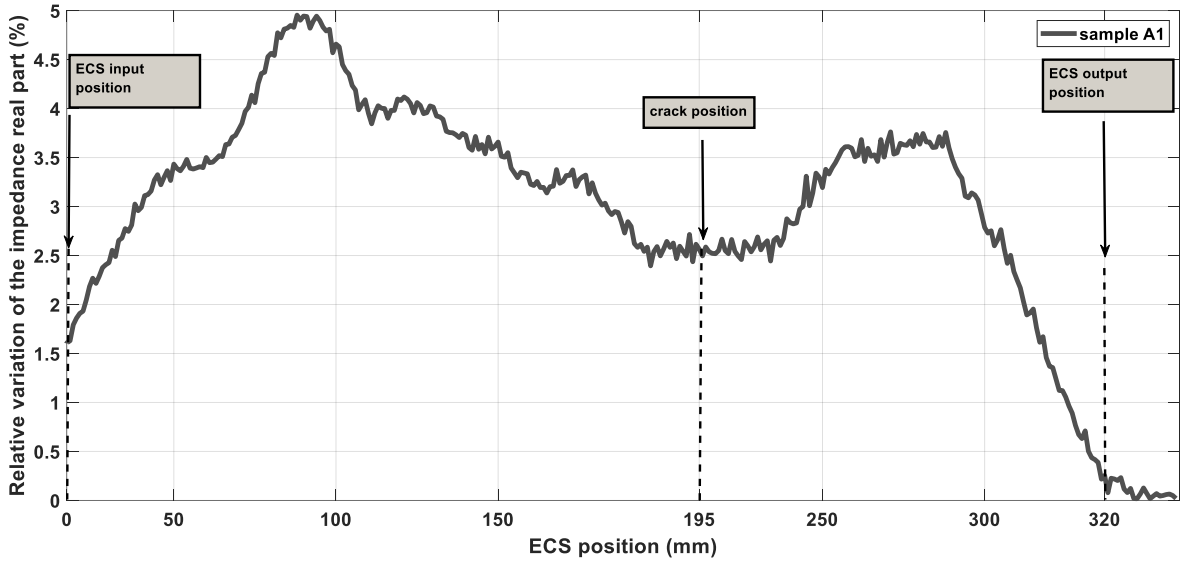

Fig. 14. ECS Impedance Real Part Changes with SFRC sample A1 according to ECS position.

Figure 14 represents the ECS Impedance Real Part Changes with SFRC sample A1 according to ECS position. The begin 0 mm and end 320 mm positions (Fig. 13) correspond to the extremities of the sample. The ruler reading correspond to the graph position with adding 17mm.

Thus, the crack is occurred at the position of **195 mm** The ECS Impedance Real Part Change at this location is notably low, measuring 2.5%, which is half of its maximum value (5%). This low value indicates a potential issue, either a lack of fibers in that area or improper fiber positioning. Additionally, it is noteworthy that the zone of low ECS Impedance Real Part Change measurement extends a considerable distance, approximately 37 mm. In this zone, fibers are inadequately dispersed, hindering their ability to effectively absorb stress forces, which causes the crack.

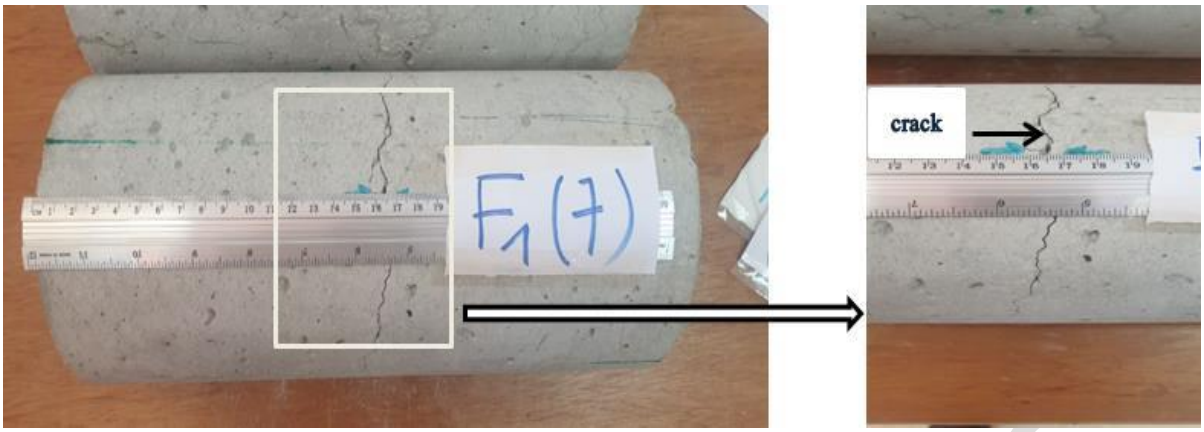

Fig. 15. SFRC sample F1(7) after undergoing the Brazilian destructive test.

In Fig. 15, SFRC sample F1(7) after undergoing the Brazilian destructive test is displayed, with the crack being measured from the top of the specimen using a ruler. The crack is positioned at 165 mm from the top.

Figure 16 illustrates the exact course of the crack in SFRC sample F1(7), which occurred approximately perpendicular to the axis of the cylindrical sample. The measured length of the crack is 23 cm.

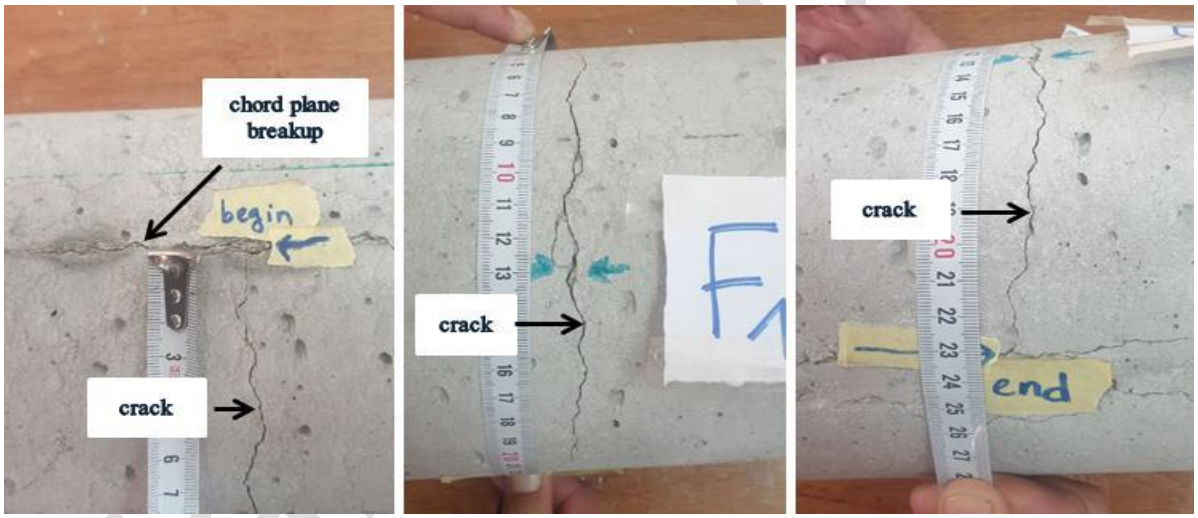

Fig. 16. Course and Length of the Crack in SFRC Sample F1(7).

Figure 17 depicts the ECS Impedance Real Part Changes with SFRC Sample F1(7). The crack position in ECS Impedance Real Part Change is located at 165mm. The impedance values are notably low, measuring 3%, dropping from the maximal values of 5%, indicating a potential issue-either a lack of fibers or improper positioning. Additionally, the zone of low variation impedance, extending around 83mm, covers a significant distance where fibers are inadequately dispersed, leaving the material vulnerable to stress forces. The mal-dispersion of fibers is identified as the cause.

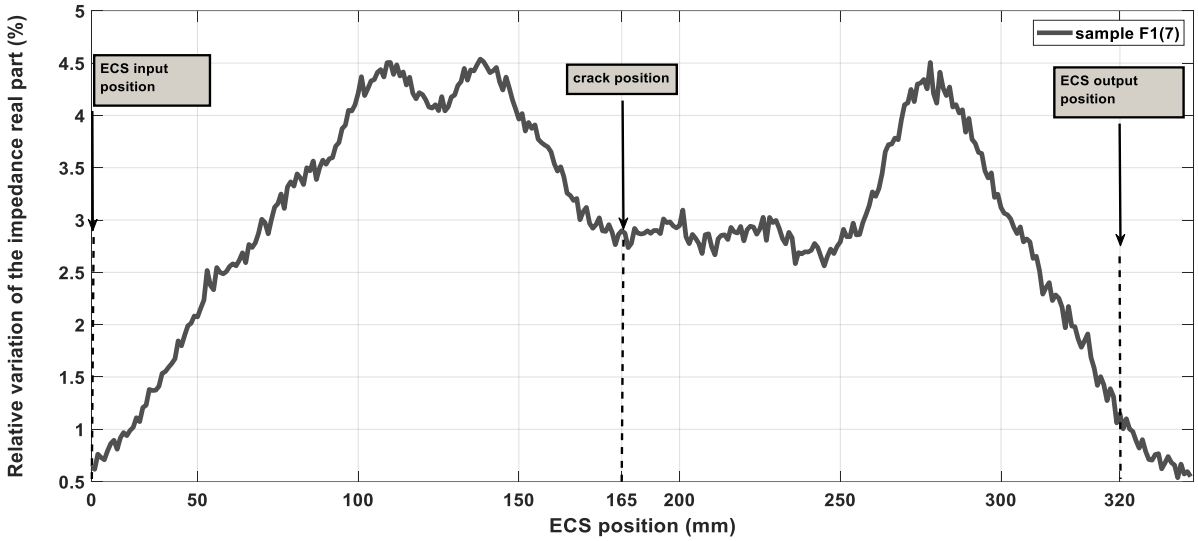

Fig. 17. ECS Impedance Real Part Changes with SFRC sample F1(7) according to ECS position.

Figure 18 illustrates the SFRC Sample F2(4) after undergoing the Brazilian destructive test, with the crack located 135 mm from the top of the specimen.

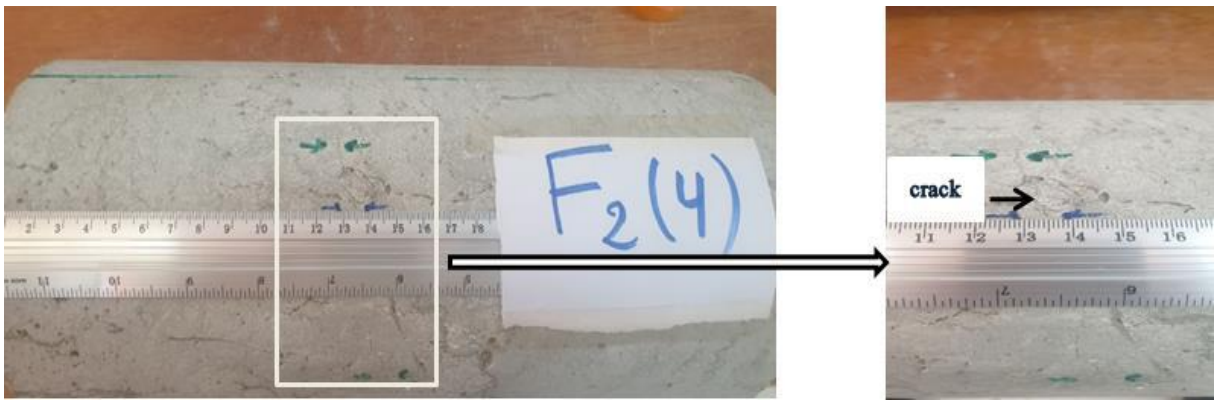

Fig. 18. SFRC sample F2(4) after undergoing the Brazilian destructive test.

Figure 19 illustrates the exact course of the crack in SFRC sample F2(4), which occurred approximately perpendicular to the axis of the cylindrical sample. The measured length of the crack is17 cm.

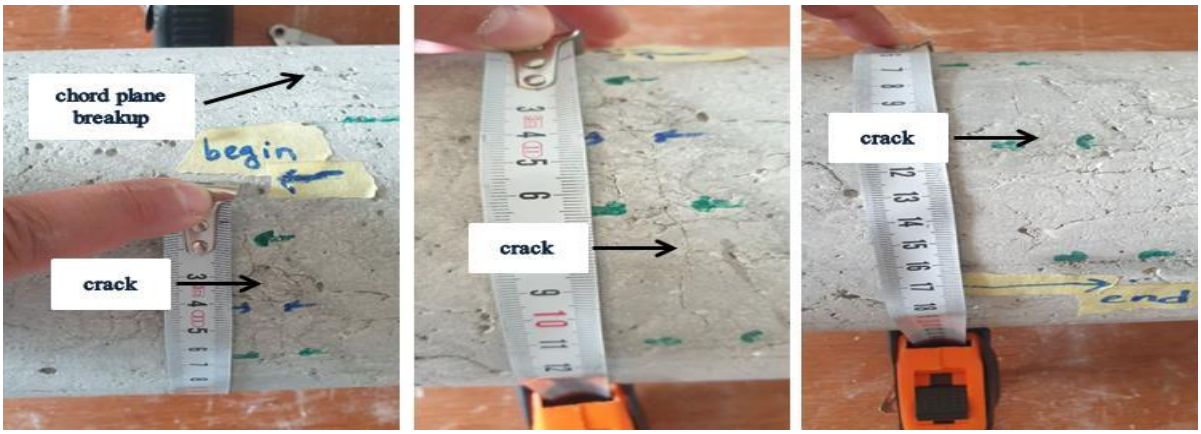

Fig. 19. The Course and Length of the Crack in SFRC Sample F2(4).

Figure 20 illustrates ECS Impedance Real Part Changes with SFRC Sample F2(4), showing the crack position at 135 mm. The impedance change values are notably low, measuring 1.8%, approximately half of the maximal impedance value of 3.2%, indicating mal-dispersion of fibers as the cause for the crack development in that zone. The zone of low variation impedance extends around 200mm, covering a substantial distance where fibers are inadequately dispersed, rendering the material vulnerable to stress forces and causing the development of the crack in that zone.

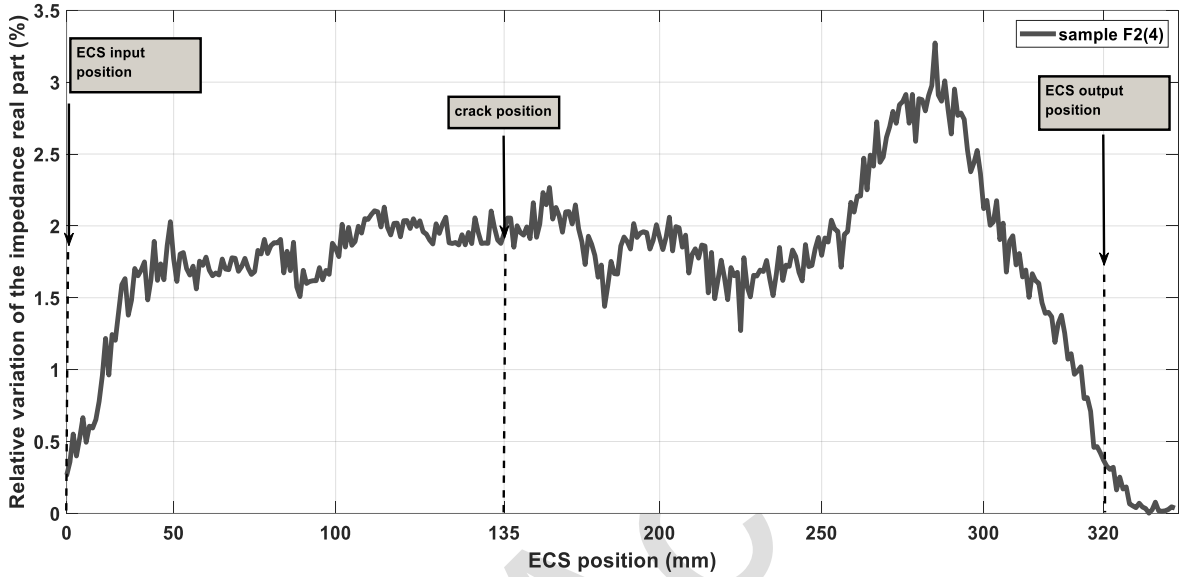

Fig. 20. ECS Impedance Real Part Changes with SFRC sample F2(4) according to ECS position.

Figure 21 depicts ECS Impedance real part changes with SFRC sample A5 that did not develop cracks following the Brazilian destructive testing.

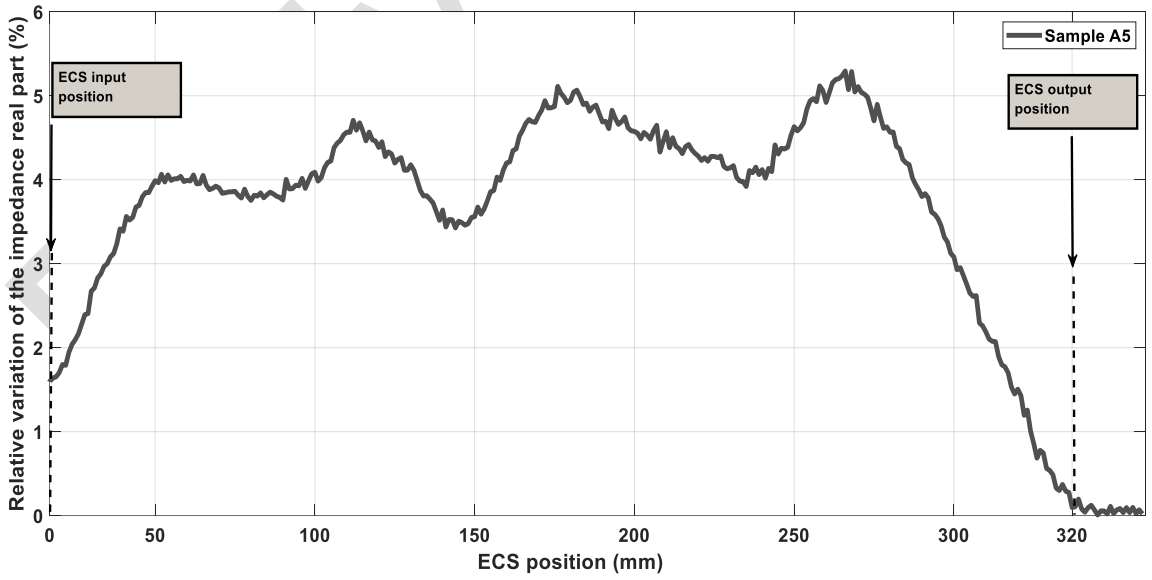

Fig. 21. ECS Impedance Real Part Changes with SFRC sample A5 according to ECS position.

The impedance measurement ranges between 4% and 5%, with a slight decrease observed at 150 mm, reaching a value of 3.5%. It quickly rises again to a value of 4%.

The absence of cracks in this area is attributed to the absence of significant low variation impedance zones. Furthermore, the value of 3.5% did not extend over a long distance, indicating

that the fibers are possibly inadequately distributed, covering only 10 mm. Additionally, the zones with a high variation impedance in the vicinity of the vulnerable area (with a low variation impedance) lead to the absorption of stress energy, potentially exacerbating the risk of crack formation.

It is notable that all samples that did not develop cracks share the same signature as shown in Fig. 18.

In this part, one has seen that vulnerable areas are identified where cracks are observed during the destructive test and confirmed with a direct visual. These cracks are associated either with a lack of fibers in the area or poor fiber placement.

The impedance change signature given by the non-destructive eddy current scanning system confirms the presence of these vulnerable zones susceptible to cracking, which are described by the wide areas of low impedance variation. Thus, the correlations between the impedance change signature and the Brazilian signature allow to confirm the feasibility of the crack prediction without carrying out the destructive tests.

Since the fiber volume fraction remains constant at 1 percent for all groups, cracks occurred in only three samples due to fiber distribution within the concrete. In these samples, the fiber distribution was irregular, leading to zones of vulnerability where cracks develop under stress. Conversely, in the 30 remaining samples, the fiber distribution has been more uniform, preventing cracks from developing.

Correlation between crack zones and impedance change signatures was carried out successively. This has enabled us to assert that cracking only occurs in zones with the lowest impedance values and the widest extent of these zones. These cracks are approximately along the axis perpendicular to the cylinder.

The proposed approach therefore enables crack formation to be predicted on the basis of the criterion of the lowest impedance zone and its widest extent.

6. Conclusion

In this paper one has presented an eddy current non-destructive testing method with automated scan system, intended for evaluation of the steel fiber distribution, in order to predict cracks in *Steel Fiber Reinforced Concrete* (SFRC).

The proposed method is successfully applied on samples with known fiber distribution. The impedance change signature shows clearly the highest and lowest of the fiber volume fractions along the samples, thus its effectiveness is approved. This method has proved effective in distinguishing different zones with varying volume fractions in the same sample.

Its application on the samples with random fiber distribution shows a robust correlation between the measured impedance changing and the observed cracks on the SFRC samples after undergoing the Brazilian destructive test. Vulnerable areas are identified where cracks are visually observed during the Brazilian destructive test. These cracks are associated either with a lack of fibers in the area or poor fiber orientation, where wide zones with low variation impedance and extended low-variation impedance are observed.

Out of 33 tested samples, only 3 showed cracks. On these 3 samples, non-destructive testing revealed a wide zone of low and extended impedance variation. For the rest of the samples, no cracks were observed, even though the impedance variation signature showed areas of low impedance variation but with small widths. Additionally, these areas are surrounded by zones of high impedance variation allow to absorb the energy of the stresses, potentially exacerbating the risk of crack formation.

The correlations between the impedance change signature and the Brazilian test results allow to confirm the feasibility of the crack prediction without carrying out the destructive tests. This

approach proves instrumental in identifying vulnerable areas susceptible to crack development within the SFRC.

Acknowledgment

The authors would like also to acknowledge the laboratory engineers of the civil engineering department, sciences and applied science faculty, Bouira university, for their help.

The investigations in this paper were conducted within the framework of DGRSDT for doctoral student and they are part of the PRFU research project (Project number: A01L07UN100120190001).

Reference

[1] Altun, F., Haktanir, T., & Ari, K. (2007). Effects of steel fiber addition on mechanical properties of concrete and RC beams. *Construction and Building Materials*, *21*(3), 654-661. https://doi.org/10.1016/j.conbuildmat.2005.12.006

[2] Li, H., Wu, Y., Zhou, A., Lu, F., Lei, Z., Zeng, B., & Zhu, K. (2023). Cracking pattern and bearing capacity of steel fiber-reinforced concrete single-layer tunnel lining. *Sustainability*, *15*(13), 10665. https://doi.org/10.3390/su151310665

[3] Su, Q. (2020). Strengths of recycled concrete added with steel fiber. Archives of Civil Engineering, *66*(3). https://doi.org/10.24425/ace.2020.134421

[4] Krassowska, J., & Kosior-Kazberuk, M. (2019). Experimental investigation of shear behavior of two-span fiber reinforced concrete beams. *Archives of Civil Engineering*, *65*(2). https://doi.org/10.2478/ace-2019-0017

[5] Gettu, R., Gardner, D. R., Saldivar, H., & Barragán, B. E. (2005). Study of the distribution and orientation of fibers in SFRC specimens. *Materials and Structures*, *38*, 31-37. https://doi.org/10.1007/BF02480572

[6] Zhang, S., Liao, L., Song, S., & Zhang, C. (2018). Experimental and analytical study of the fibre distribution in SFRC: a comparison between image processing and the inductive test. *Composite Structures*, *188*, 78-88. https://doi.org/10.1016/j.compstruct.2018.01.006

[7] Tiberti, G., Minelli, F., Plizzari, G. A., & Vecchio, F. J. (2014). Influence of concrete strength on crack development in SFRC members. *Cement and Concrete Composites*, *45*, 176-185. https://doi.org/10.1016/j.cemconcomp.2013.10.004

[8] Lee, J. H. (2017). Influence of concrete strength combined with fiber content in the residual flexural strengths of fiber reinforced concrete. *Composite Structures*, *168*, 216-225. https://doi.org/10.1016/j.compstruct.2017.01.052

[9] Abrishambaf, A., Barros, J. A., & Cunha, V. M. (2013). Relation between fibre distribution and post-cracking behaviour in steel fibre reinforced self-compacting concrete panels. *Cement and Concrete Research*, *51*, 57-66. https://doi.org/10.1016/j.cemconres.2013.04.009

[10] Akkaya, Y., Shah, S. P., & Ankenman, B. (2001). Effect of fiber dispersion on multiple cracking of cement composites. *Journal of Engineering Mechanics*, *127*(4), 311-316. https://doi.org/10.1061/(ASCE)0733-9399(2001)127%3A4(311)

[11] Bordelon, A. C., & Roesler, J. R. (2014). Spatial distribution of synthetic fibers in concrete with X-ray computed tomography. *Cement and Concrete Composites*, *53*, 35-43. https://doi.org/10.1016/j.cemconcomp.2014.04.007

[12] Liu, J., Li, C., Liu, J., Cui, G., & Yang, Z. (2013). Study on 3D spatial distribution of steel fibers in fiber reinforced cementitious composites through micro-CT technique. *Construction and Building Materials*, *48*, 656-661. https://doi.org/10.1016/j.conbuildmat.2013.07.052

[13] Park, T., Her, S., Jee, H., Yoon, S., Cho, B., Hwang, S. H., & Bae, S. (2021). Evaluation of orientation and distribution of steel fibers in high-performance concrete column determined via micro-computed tomography. *Construction and Building Materials*, *270*, 121473. https://doi.org/10.1016/j.conbuildmat.2020.121473

[14] Fladr, J., Bily, P., & Broukalova, I. (2019). Evaluation of steel fiber distribution in concrete by computer aided image analysis. *Composite Materials and Engineering*, *1*(1), 49-70. https://doi.org/10.12989/cme.2019.1.1.049

[15] Ďubek, M., Makýš, P., Ďubek, S., & Petro, M. (2018). The evaluation of the content of fibers in steel fiber reinforced structures and image analysis. *Journal of Civil Engineering and Management*, *24*(3), 183-192. https://doi.org/10.3846/jcem.2018.1642

[16] Ozyurt, N., Mason, T. O., & Shah, S. P. (2006). Non-destructive monitoring of fiber orientation using AC-IS: An industrial-scale application. *Cement and Concrete Research*, *36*(9), 1653-1660. https://doi.org/10.1016/j.cemconres.2006.05.026

[17] Faifer, M., Ottoboni, R., Toscani, S., & Ferrara, L. (2010, May). Steel fiber reinforced concrete characterization based on a magnetic probe. In *2010 IEEE Instrumentation & Measurement Technology Conference Proceedings* (pp. 157-162). https://doi.org/10.1109/IMTC.2010.5488179

[18] Torrents Dolz, J. M., Juan Garcia, P., Patau, O., & Aguado de Cea, A. (2009). Surveillance of steel fibre reinforced concrete slabs measured with an open-ended coaxial probe. In *XIX IMEKO World Congress. Fundamental and Applied Metrology* (pp. 2282-2284). http://www.imeko2009.it.pt/Papers/FP_633.pdf

[19] Lataste, J. F., Behloul, M., & Breysse, D. (2008). Characterisation of fibres distribution in a steel fibre reinforced concrete with electrical resistivity measurements. *NDT & E International*, *41*(8), 638-647. https://doi.org/10.1016/j.ndteint.2008.03.008

[20] Cavalaro, S. H. P., López, R., Torrents, J. M., & Aguado, A. (2015). Improved assessment of fibre content and orientation with inductive method in SFRC. *Materials and Structures*, *48*, 1859-1873. https://doi.org/10.1617/s11527-014-0279-6

[21] Cavalaro, S. H., López-Carreño, R., Torrents, J. M., Aguado, A., & Juan-García, P. (2016). Assessment of fibre content and 3D profile in cylindrical SFRC specimens. *Materials and Structures*, *49*, 577-595. https://doi.org/10.1617/s11527-014-0521-2

[22] Torrents, J. M., Blanco, A., Pujadas, P., Aguado, A., Juan-García, P., & Sánchez-Moragues, M. Á. (2012). Inductive method for assessing the amount and orientation of steel fibers in concrete. *Materials and Structures*, *45*, 1577-1592. https://doi.org/10.1617/s11527-012-9858-6

[23] Gherdaoui, L., Bensaid, S., Trichet, D., Houassine, H., & Saoudi, N. (2023). Complex Magnetic Permeability Evaluation of Steel Fibers Using Eddy Current NDE and Inverse Problem Methods. *Progress in Electromagnetics Research Letters*, *113*. https://doi.org/10.2528/PIERL23090804

Loukmane Gherdaoui was born at Medea, Algeria. He is a PHD student at Bouira University. His research interests lie in Electromagnetic and Eddy Current Nondestructive Testing.

Nacira Saoudi, receiving engineering degree in civil engineering VOA in 2001 from USTHB, Algers, and her Ph.D from Boumerdes University. She has worked as supervisor of projects. Actually she is is an assistant professor of civil engineering at Bouira University, Algeria. Her research activities focus on the development of new materials, simulation and modeling of material behavior, non-destructive testing.

Hamza Houassineh obtained his PhD from the University of Mouloud MAMMERI in Tizi Ouzou, Algeria, in 2010. He is currently a professor in the Electrical Engineering Department at the University of Bouira, Algeria. His research interests encompass the diagnosis of electrical equipment, characterization of dielectric and magnetic materials, surge voltage, and energy quality.

Samir Bensaid was born in 1972 at Timizart, Tizi-Ouzou, Algeria. He received his State Engineer degree in 1996 from INHC Boumedres, Algeria, and his Ph.D. degree in 2006 from Nantes University, France. He is currently a full Professor of Electrical Engineering at Bouira University, Algeria. He specializes in Electromagnetic and Eddy Current Nondestructive Testing & Evaluation measurements and modeling of conventional and non-conventional materials. He also works on the design and diagnosis of electrical devices.

Metrol. Meas. Syst., Vol. 31 (2024), No. 4
DOI: 10.24425/mms.2024.152047

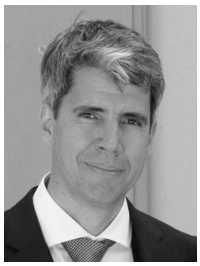

Didier Trichet, MSc, PhD (M), was born in 1970 at Saint Malo, France. He received the M.S. and Ph.D. degrees in Electrical Engineering from Nantes University, France, in 1999. He is currently a full Professor at Polytech'Nantes, former head of Master 2 Electrical Energy international program of Nantes University and director of IREENA laboratory since January 2022. He specializes on advanced numerical modelling of multi-physic and multi-scale electromagnetic phenomena of low frequency devices, electro thermal processes, Non-Destructive Testing and diagnosis of complex electrical structures, high-efficiency fuel cell power train and advanced power electronics. He is associate editor for IEEE Transaction on Magnetics.